ACI STRUCTURAL JOURNAL TECHNICAL PAPER

Title no. 108-S26

Failure Mode Transitions in Reinforced Concrete Beams—Part 1: Theoretical Model

by Alberto Carpinteri, Jacinto Ruiz Carmona, and Giulio Ventura

The bridged crack model is an efficient theoretical and numerical tool for investigating the behavior of structural reinforced concrete (RC) elements in bending. The model is based on linear elastic fracture mechanics concepts and equilibrium and compatibility equations are applied to a Mode I cracked beam segment. The model is herein extended to include both compression crushing and shear cracking, assuming a shape for the hypothetical crack trajectory and determining the shear crack initiation point and the load versus crack depth propagation curve. In this paper, the three collapse mechanisms—flexure, shear, and crushing—are considered jointly, so that failure modes can be immediately compared to detect which one dominates and the related failure load. Consequently, the model predicts all the mutual transitions between the different mechanisms, and these transitions are shown by varying the governing nondimensional parameters. A global transition scheme is introduced for illustrating the relevant size/scale effects.

Keywords: failure; scale; shear.

INTRODUCTION

A vast amount of literature exists separately on reinforced concrete (RC) beams models involving the three possible failure mechanisms: flexure, shear, and crushing. The study of the transitions between these mechanisms inside a consistent theoretical framework, however, is still an open question, especially with reference to the experimentally known size effects. One of the earliest contributions in the field is the paper by Kani,[1] aimed to "establish...a rational theory" to flexural and diagonal tension failures and their transition. While Kani's model[1] is based on the hypothesis of the formation of internal resisting substructures in the beam, the main issue for the present analysis is to get a joint consistent modeling of the aforementioned three failure mechanisms inside the theoretical frame of fracture mechanics.

Shear crack propagation and diagonal tension failure have been addressed in the literature by several authors with different approaches. For example, some analyses with cohesive crack modeling have been published by Gustafsson,[2] Gustafsson and Hillerborg,[3] and Niwa.[4,5] In the framework of linear elastic fracture mechanics, some models are especially remarkable due to some similarities with the present approach. In particular, Jenq and Shah[6] analyzed the diagonal shear fracture superposing the contribution of concrete and steel bars with a technique that is somehow conceptually close to the bridged crack model by Carpinteri[7,8] for the pure flexural (steel yielding) failure. Some further developments of this approach with other original contributions were made by So and Karihaloo[9] and Karihaloo.[10]

The bridged crack model was proposed by Carpinteri[7,8] for the study of RC beams by fracture mechanics. Size effect and ductile-brittle transition were analyzed to determine the minimum amount of reinforcement.[11-14] Then, a first extension to cohesive stresses was presented,[15] as well as a model combining cohesive stresses and reinforcing bars.[16,17] The model has then been further extended analyzing concrete crushing and flexural failures.[18] Moreover, whereas limit state analyses yield only the ultimate load, the bridged crack model may in addition reveal scale effects, instability phenomena, and ductile-brittle failure transitions of the structural member.

In this paper, RC beams without stirrups are analyzed. To extend the bridged crack model to account for the shear cracks formation and to evaluate the diagonal tension failure load, some hypotheses about the crack trajectory and the evaluation of the stress-intensity factors are added, as well as a criterion for concrete crushing based on the maximum stress at the extrados. A unified general model is obtained, so the study of the transitional phenomena is naturally accomplished. The model is analyzed by showing the influence of the variation in the nondimensional parameters on the mechanical response and a global failure mode transition scheme is introduced.

RESEARCH SIGNIFICANCE

Vast literature exists on collapse mechanisms of beams, but an established model joining flexural, shear, and crushing failures is missing. Herein, the three phenomena are read under the same conceptual scheme, allowing for a direct relation between the failure modes. Moreover, whereas the majority of shear failure models assume both the shape and the initiation point for the critical crack, herein the crack initiation is found based on the stability of the cracking process. Although linear elastic fracture mechanics is used in the present paper, a similar model could be developed in the hypothesis of nonlinear cohesive cracks.

MODELING FLEXURAL AND SHEAR CRACKS

In this paper, the problem of determining the carrying capacity of a beam is solved by a fracture mechanics analysis. A family of crack paths is considered. For each one, the stability of the fracturing process and the load required to activate it are evaluated. Then, the minimum load giving unstable crack propagation is assumed as the failure load and the corresponding crack path as determining the collapse mechanism. Therefore, the model will be adequate for sufficiently slender beams not developing direct strutting.[1]

Consider a cracked beam (Fig. 1) and assume a crack propagation condition ruled by the comparison of the stress-

ACI Structural Journal, V. 108, No. 3, May-June 2011.
MS No. S-2007-253.R3 received April 1, 2010, and reviewed under Institute publication policies. Pertinent discussion including author's closure, if any, will be published in the March-April 2012 *ACI Structural Journal* if the discussion is received by November 1, 2011.

Alberto Carpinteri *has been a Full Professor of structural mechanics at the Politecnico di Torino, Torino, Italy, since 1986. He received doctoral degrees in nuclear engineering and mathematics from the University of Bologna, Bologna, Italy, in 1976 and 1981, respectively.*

Jacinto Ruiz Carmona *is a Research Assistant in solid mechanics and materials science at the University of Castilla-La Mancha (UCLM), Castilla-La Mancha, Spain. He received his degree in civil engineering from Madrid Polytechnical University, Madrid, Spain, and his PhD in solid mechanics from UCLM in 2000 and 2006, respectively. His research interests include the fracture of plain and reinforced concrete.*

Giulio Ventura *is an Associate Professor of structural mechanics at the Politecnico di Torino. He received his MS in civil engineering and his PhD in structural engineering from the University of Catania, Catania, Italy, in 1990 and 1994, respectively. His research interests include computational mechanics and reinforced concrete theoretical and experimental research.*

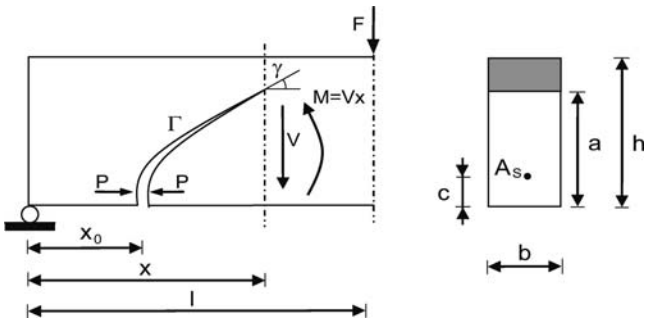

Fig. 1—Cracked beam.

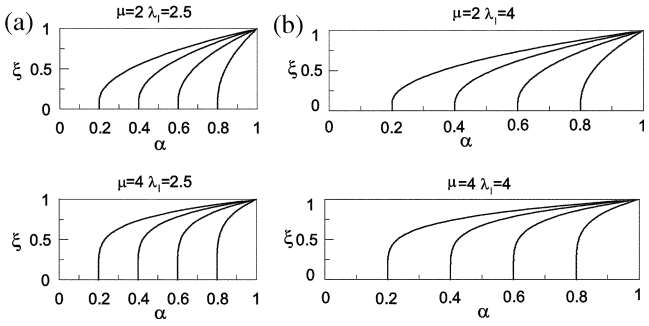

Fig. 2—Normalized crack trajectories: (a) $\lambda_1 = 2.5$; and (b) $\lambda_1 = 4$.

intensity factor (SIF) K_I to the concrete toughness K_{IC}. Handbooks[19] report linear elastic fracture mechanics (LEFM) solutions for Mode I (bending) fracture. In the case of Fig. 1, however, no SIF data are available and approximate expressions will be derived as described in the following.

In Fig. 1, all symbols used are defined: the section width b and depth h, the crack tip vertical and horizontal position a and x, the crack mouth horizontal position x_0, and the shear span l. The corresponding nondimensional quantities are introduced after dividing by the beam depth h, the vertical distances, and by the shear span l, the horizontal distances. Then, $\alpha = x/l$ is the horizontal distance of the crack tip from the support, $\xi = a/h$ is the crack depth, $\alpha_0 = x_0/l$ is the initial crack mouth position, $\zeta = c/h$ is the reinforcement cover, and $\lambda_l = l/h$ is the shear span slenderness ratio.

The crack trajectory Γ is split into two parts: a vertical segment Γ_1, extending from the bottom to the reinforcement layer, and a power-law curve Γ_2, going from the end of the first part (reinforcement layer) to the loading point. Its analytical definition is

$$\alpha(\zeta, \xi) = \begin{cases} \alpha_0 & 0 \le \xi \le \zeta \\ \alpha_0 + \left(\dfrac{\xi - \zeta}{1 - \zeta}\right)^{\mu}(1 - \alpha_0) & \zeta \le \xi \le 1 \end{cases} \quad (1)$$

Some crack trajectories are drawn in Fig. 2. Note that the peculiarity of the present approach, compared to the literature, is that the crack initiation point will be determined by analyzing the crack propagation process stability, whereas the shape is modeled by the parameter μ based on experimental results, as discussed in the companion paper.[20]

With reference to Fig. 1, let K_I be the SIF at the crack tip, given by the sum of the SIF K_{IV} due to the bending moment associated to the shear force V, and K_{IP} due to the closing force applied by the reinforcing bars. The crack propagation condition reads

$$K_I = K_{IV} - K_{IP} = K_{IC} \quad (2)$$

The value of K_{IC} in Eq. (2) may be determined by the RILEM recommendations[21,22] or derived by the procedures suggested by Abdalla and Karihaloo[23] and Karihaloo and Abdalla.[24]

To approximate K_{IV}, Jenq and Shah[6] assumed that it can be evaluated by the SIF of a beam with a straight vertical crack subjected to the bending moment at the cross section containing the mouth of the crack. Here, a similar approach is followed, but the bending moment at the section where the crack tip is located is considered

$$K_{IV} = \frac{Vl\alpha(\zeta, \xi)}{h^{3/2}b} Y_M(\xi) = \frac{V}{h^{1/2}b} Y_V(\zeta, \xi)\lambda_l \quad (3)$$

where the function Y_M is given by a handbook solution.[16,19] An approximate expression for the SIF K_{IP} at the crack tip due to the reinforcement reaction P is derived from the case of a vertical straight crack. Several numerical analyses by boundary elements[25] have been performed to evaluate the SIF for different positions of the crack tip. It is observed that the SIF is mainly a function of the angle γ defined in Fig. 1 and that K_{IP} can be approximated as

$$K_{IP} = \frac{P}{h^{1/2}b} Y_P(\zeta, \xi)\beta(\gamma) = \frac{P}{h^{1/2}b} Y_{P_\gamma}(\zeta, \xi) \quad (4)$$

where given γ in degrees by a nonlinear data fit it is

$$\beta(\gamma) = \left(\frac{\gamma}{90}\right)^{0.2} \quad (5)$$

and $Y_{P_\gamma} = Y_P(\zeta, \xi)\beta(\gamma)$. Function $Y_P(\zeta, \xi)$ can be found in fracture mechanics handbooks.[16,19] Therefore, by accurate numerical analyses, the exact values for the SIFs were evaluated, validating Eq. (3) and allowing to define Eq. (4) by data fitting. Let $\rho = A_s/bh$ be the reinforcement percentage referred to the entire cross section, w the crack opening at the reinforcement position, and

$$N_P = \frac{\sigma_y h^{1/2}}{K_{IC}}\rho \tag{6}$$

the brittleness number defined by Carpinteri.[7] The result of substituting Eq. (3) and (4) into Eq. (2) is

$$\tilde{V}_F = \frac{1}{\lambda_l Y_V(\xi)}[1 + N_P \tilde{P} Y_{P_\gamma}(\zeta, \xi)] \tag{7}$$

where

$$\tilde{V}_F = \frac{V_F}{K_{IC} h^{1/2} b} \tag{8}$$

$$\tilde{P} = \frac{P}{P_P} \tag{9}$$

and P_P is the reinforcement traction limit. A rigid-plastic constitutive equation is assumed for the reinforcement, ruled by the stress σ_y, defined as the minimum between the yielding and the sliding stress for the bars.[7,8] Then, $P_P = A_s\sigma_y$, where A_s is the reinforcement area. Equation (7) gives the shear of crack propagation as a function of the bar traction stress σ_s, depending on the crack opening w at the reinforcement. Note that the stiffness of the flexural reinforcement is not expected to give a significant contribution to the shear strength due to the absence of stirrups in the present model.

Let E be the concrete Young's modulus and $\tilde{w}$ the nondimensional crack opening at the reinforcement

$$\tilde{w} = \frac{wE}{K_{IC} h^{1/2}} \tag{10}$$

The crack opening $\tilde{w}$ at the nondimensional coordinate ζ (at the reinforcement), evaluated for the crack propagation shear $V = V_F$, can be determined[7,8] by adding the two contributions of the shear $\tilde{V}$ and the bar reaction $\tilde{P}$

$$\begin{aligned}\tilde{w} = \tilde{w}_V - \tilde{w}_{P_\gamma} = 2\lambda_l \tilde{V}_F \int_\zeta^\xi Y_V(z) Y_{P_\gamma}(\zeta, z) g(\zeta, z) dz \\ - 2N_P \tilde{P} \int_\zeta^\xi Y_{P_\gamma}^2(\zeta, z) g(\zeta, z) dz\end{aligned} \tag{11}$$

where $g(\zeta,\xi)$ is the Jacobian mapping the curvilinear integral along the crack trajectory onto the interval $[0,\xi]$

$$g(\zeta, \xi) = \begin{cases} 1 & \xi < \zeta \\ \sqrt{\mu^2 \lambda_l^2 \left(\frac{1}{1-\zeta}\right)^{2\mu} (\xi - \zeta)^{2(\mu-1)} (1-\alpha_0)^2 + 1} & \xi \geq \zeta \end{cases} \tag{12}$$

According to the rigid-perfectly plastic assumption, it is $\tilde{w} = 0$ up to the yielding or slippage of the reinforcement, so that a displacement compatibility condition allows to determine $\tilde{P}$ as a function of $\tilde{V}$. From Eq. (11)

$$r''(\zeta, \xi) = \frac{\lambda_l \tilde{V}_F}{N_P \tilde{P}} = \frac{\int_\zeta^\xi Y_{P_\gamma}^2(\zeta, z) g(\zeta, z) dz}{\int_\zeta^\xi Y_V(z) Y_{P_\gamma}(\zeta, z) g(\zeta, z) dz} \tag{13}$$

where $\tilde{V}_P$ is the value of $\tilde{V}_F$ at the reinforcement traction limit ($P = P_P$). If $\tilde{V}_F < \tilde{V}_P$, from Eq. (7) and (13), it is

$$\tilde{V}_F = \frac{1}{\lambda_l \left[Y_V(\xi) - \frac{Y_{P_\gamma}(\zeta, \xi)}{r''(\zeta, \xi)} \right]} \tag{14}$$

If $\tilde{V}_F = \tilde{V}_P$, from Eq. (7), it is

$$\tilde{V}_P = \frac{1}{\lambda_l Y_V(\xi)}[1 + N_P Y_{P_\gamma}(\zeta, \xi)] \tag{15}$$

Therefore, according to the model, when $\tilde{V}_F < \tilde{V}_P$, the shear of crack propagation $\tilde{V}_F$ depends only on the crack depth ξ and is not affected by the brittleness number N_P. In the present model, the beam behavior up to failure described assumes the crack depth—the only monotonically increasing quantity in the process—as the control parameter. Equations (14) and (15) give the shear respecting: a) equilibrium; b) compatibility; and c) incipient crack propagation (SIF equal to the toughness of the material).

MODELING CONCRETE CRUSHING

The linear elastic fracture mechanics approach followed in the derivation of the present model allows for the immediate determination of the stresses and their combination based on the superposition principle. Therefore, the concrete crushing criterion is assumed to be stress-based. Concrete crushing is detected by comparing the maximum compressive stress (located by linear elasticity at the uppermost edge of the cracked section) to a conventional crushing strength σ_{cu}. If it is assumed that the linear elastic fracture mechanics shape functions represent strains, however, a strain-based crushing criterion can be introduced as well through a fictitious crushing stress given by the assumed crushing strain times the modulus of elasticity.

The maximum compressive stress is expressed as the sum of a term due to the shear V (that is, to the bending moment at the cross section containing the crack tip) and a term due to the reinforcement reaction P

$$\sigma_c = \sigma_c^V + \sigma_c^P \tag{16}$$

Adaptive finite element computations on cracked sections[18] and nonlinear regressions allowed to determine numerically two functions $Y_\sigma^M(\xi)$ and $Y_\sigma^P(\zeta, \xi)$, so that the contributions to σ_c from V and P can be written as

$$\sigma_c^V = \frac{M}{bh^2} Y_\sigma^M(\xi) = \frac{Vl\alpha(\zeta, \xi)}{bh^2} Y_\sigma^M(\xi) = \lambda_l \frac{V}{bh} Y_\sigma^V(\xi) \tag{17}$$

$$\sigma_c^P = -\frac{P}{bh} Y_\sigma^P(\zeta, \xi) \tag{18}$$

where $Y_\sigma^V(\xi) = \alpha(\zeta, \xi) Y_\sigma^M(\xi)$. The result of substituting Eq. (17) and (18) into Eq. (16) is

$$\sigma_c = \lambda_l \frac{V}{bh} Y_\sigma^V(\xi) - \frac{P}{bh} Y_\sigma^P(\zeta, \xi) \tag{19}$$

Let $V = V_C$ be the shear for which $\sigma_c = \sigma_{cu}$. In nondimensional form, it is

$$\frac{\sigma_{cu} h^{1/2}}{K_{IC}} = \tilde{V}_C \lambda_l Y_\sigma^{V_C}(\xi) - N_P \tilde{P} Y_\sigma^P(\zeta, \xi) \tag{20}$$

Consequently, a brittleness number for the crushing failure is defined as

$$N_C = \frac{\sigma_{cu} h^{1/2}}{K_{IC}} \tag{21}$$

so that the nondimensional crushing shear is given by

$$\tilde{V}_C = \frac{1}{\lambda_l Y_\sigma^V(\xi)} [N_C + N_P \tilde{P} Y_\sigma^P(\zeta, \xi)] \tag{22}$$

At steel yielding, it is $\tilde{P} = 1$ and therefore

$$\tilde{V}_C = \frac{1}{\lambda_l Y_\sigma^V(\xi)} [N_C + N_P Y_\sigma^P(\zeta, \xi)] \tag{23}$$

When $\tilde{P} < 1$, from Eq. (13), it is

$$\tilde{V}_C = \frac{1}{\lambda_l Y_\sigma^V(\xi)} \left[N_C + \frac{Y_\sigma^P(\zeta, \xi)}{Y_V(\xi) r''(\zeta, \xi) - Y_{P_\gamma}(\zeta, \xi)} \right] \tag{24}$$

The shear given by Eq. (23) and (24) produces, for a given crack depth ξ, the crushing stress $\sigma_c = \sigma_{cu}$ in the extrados of the beam. On the other hand, the equilibrium and compatibility conditions for a given crack depth ξ are satisfied during the crack growth by Eq. (14) and (15). Crushing failure occurs only when the nondimensional shear of crack propagation, Eq. (14) and (15), is equal to the nondimensional crushing shear, Eq. (23) and (24), respectively.

For $\tilde{V}_C = \tilde{V}_F \geq \tilde{V}_P$, it is

$$\frac{N_C + N_P Y_\sigma^P(\zeta, \xi)}{Y_\sigma^V(\xi)} = \frac{1 + N_P Y_P(\zeta, \xi)}{Y_V(\xi)} \tag{25}$$

For $\tilde{V}_C = \tilde{V}_F < \tilde{V}_P$, it is

$$\frac{N_C + \dfrac{Y_\sigma^P(\zeta, \xi)}{[Y_V(\xi) r''(\zeta, \xi) - Y_{P_\gamma}(\zeta, \xi)]}}{\lambda_l Y_\sigma^V(\xi)} = \frac{1}{Y_V(\xi) - \dfrac{Y_{P_\gamma}(\zeta, \xi)}{r''(\zeta, \xi)}} \tag{26}$$

Equations (25) and (26) determine the points of crushing failure in the nondimensional shear versus crack depth diagram.

FLEXURAL AND SHEAR CRACK PROPAGATION

The stability/instability of the cracking process is found to be affected by the initial crack position α_0. For illustrating the basic concept, reference is made to an experimental test by Bosco et al.[11] (Fig. 3(a)). To simplify the interpretation of the model, crushing failure is not considered at this stage.

According to the data in Fig. 3(a), it is $\lambda_l = 2.5$, $\zeta = 0.1$, and $N_P = 1.41$; and a fourth-order crack trajectory curve ($\mu = 4$) is assumed. Figure 3(b) through (d) shows the nondimensional shear force versus crack depth diagrams for the initial crack position α_0 in the interval [0.3, 1.0] and a sketch of the crack trajectories. Both stable or unstable crack propagation can occur.

When the initial crack position is at midspan ($<\alpha_0 = 1.0$) (Fig. 3(b)), the model coincides with the original bridged crack for beams in pure bending. The reinforcement reaction stabilizes the initially unstable crack propagation for a crack depth $\xi \geq 0.3$ and finally steel yielding takes place ($\xi \cong 0.7$).

The second plot (Fig. 3(c)), computed for an initial crack position $\alpha_0 = 0.7$, shows a similar behavior for low values of the crack depth. An unstable branch follows the stable one for a crack depth value of $\xi \cong 0.65$, leading the beam to failure. The change in the stability condition of the propagation is marked by the relative maximum at $\xi \cong 0.65$. Such a transition has been found experimentally by Carmona et al.[26] and Carmona.[27] Finally, in Fig. 3(d), for $\alpha_0 = 0.3$, the cracking process is always unstable.

These curves are useful for determining the starting point of the shear crack leading the beam to failure as the load is increased, as well as the failure load F. In between the infinite possible starting positions along the shear span, it is assumed that the failure crack (called in the following critical crack) is the crack whose initial point is such that the propagation process is always unstable (monotonically decreasing curve) and the shear $V_F = F/2$ required by this process is the lowest. This can be determined as follows: Fig. 4(a) shows a superposition of the plots for different arbitrary initial crack positions. Neglecting the singularity at the reinforcement position, each curve presents a relative maximum, with the exception of cracks near the support, which are always unstable. The thick line in Fig. 4(b) represents the crack having the property that its relative maximum is the minimum among the maxima of all curves—that is, it represents the cracking process of minimum shear for a completely unstable propagation. As each curve is relative to an initial crack position, the individuation of the critical crack curve allows to determine at the same time both the failure shear and the initial point of the failure crack.

The minimum in the shear force as the crack initiation position is changed has been also reported by Niwa[5] in a finite element study. Niwa's[5] results compare fairly well with the present model.

The nondimensional maximum shear during the cracking process is represented in Fig. 5, changing the location of the crack initiation α_0 and the crack path exponent μ for a fixed slenderness $\lambda_l = 2.5$. A range of μ between 4 and 8 fits the range of experimental results. For each case, a minimum load exists and for all the curves the zone where the critical shear crack develops is approximately at $0.4 < \alpha_0 < 0.7$, as shown experimentally by Kim and White.[28,29] A study of the

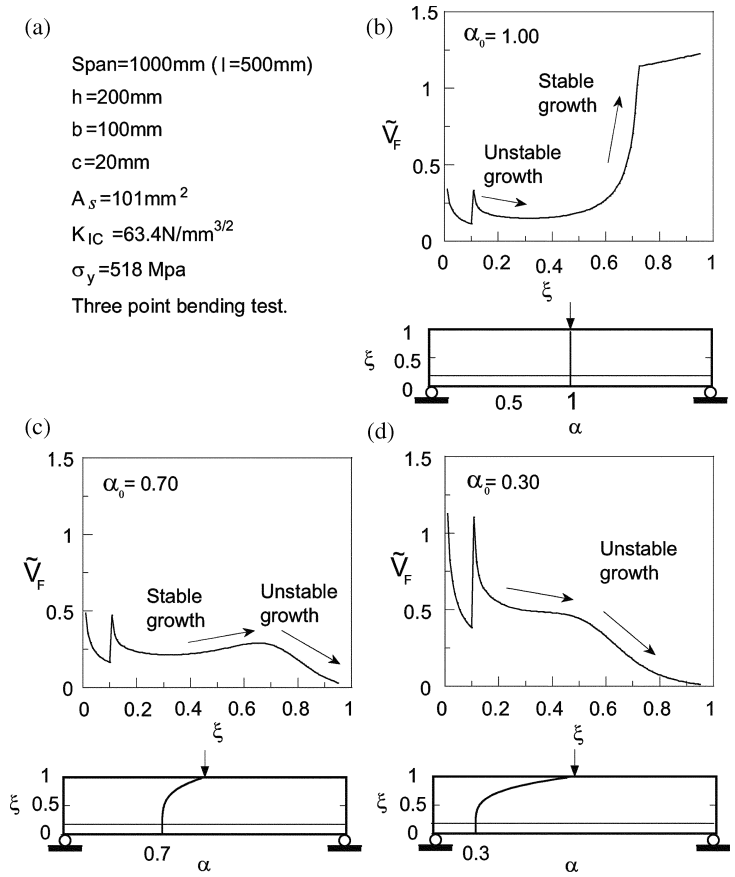

Fig. 3—Shear force versus crack depth: (a) material properties and beam geometry; (b) initial crack position α_0 = 1.00; (c) initial crack position α_0 = 0.70; and (d) initial crack position α_0 = 0.30. (Note: 1 mm = 0.0394 in.; 1 mm^2 = 0.00155 in.^{2}; 1 N = 0.225 lb; and 1 MPa = 145 psi.)

value to be given to the crack path exponent is the topic of the companion paper,[20] where an experimental program for the validation of the present model is presented.

CRUSHING FAILURE

As previously stated, the crushing points are defined as the intersection points of the crushing curve, Eq. (23) and (24), with the crack propagation curve, Eq. (14) and (15). For simplicity, this is shown graphically in the hypothesis that failure by crushing occurs at the central crack (α_0 = 1.0), although the model is not limited to this situation.

In Fig. 6, the thick curve represents the nondimensional shear of crack propagation V_F. The other family of curves represents the crushing shear V_C for different values of N_C, Eq. (23) and (24).

As seen in Fig. 6(a), given N_P = 0.25, if N_C is less than 2 (refer to the two lowest curves), crushing shear is always lower than the shear of crack propagation, and crushing precedes crack propagation, so that cracking cannot take place. For N_C = 5, the crushing curve intersects the crack propagation curve before steel yielding (point of discontinuity in the thick line), so that the collapse of the beam is by concrete crushing. For N_C > 10, the beam exhibits at first yielding ($\xi \cong 0.5$), and then crushing occurs.

In Fig. 6(b), the beam brittleness number N_P is increased to 1.0. For all the examined values of N_C, crushing occurs before steel yielding. Therefore, a variation in the brittleness numbers N_C and N_P can change the collapse mechanism from yielding to crushing and vice versa.

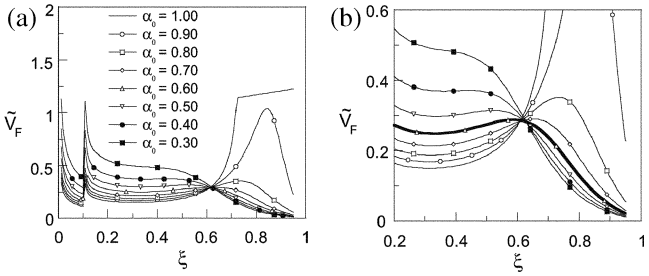

Fig. 4—(a) Shear force $\tilde{V}_F$ versus crack depth ξ; and (b) detail (thick line is curve of minimum critical shear load).

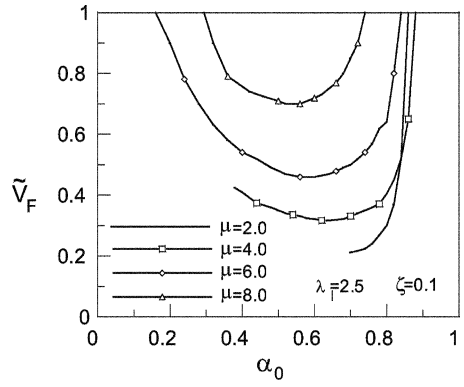

Fig. 5—Failure shear versus crack initiation position by varying μ.

TRANSITION BETWEEN DIFFERENT FAILURE MODES

The proposed model covers the three fundamental failure mechanisms of RC beams: steel yielding (flexural), diagonal tension (shear), and concrete crushing. The transitions between the aforementioned mechanisms is ruled by the nondimensional parameters N_P, N_C, and λ_l. For the sake of clarity, at first the transition from flexural to shear failure is analyzed, and then the transition from shear to crushing is considered.

Figure 7 shows four $\tilde{V}_F$ versus ξ diagrams obtained by increasing the brittleness number N_P from 0.2 to 1.0 and letting $\lambda_l = 2.5$, $\zeta = 0.1$, and $\mu = 6$. A sketch illustrating the crack trajectories at failure is reported for each beam model.

In Fig. 7(a), when the nondimensional shear force reaches a value of 0.14, the flexural crack ($\alpha_0 = 1.00$) begins its stable growth. As the load is increased, some other stable neighboring cracks develop. The marked lines in the plot represent the growing cracks. When the nondimensional shear force is equal to 0.18, the steel yields at the flexural crack: it is assumed this value represents the flexural failure load. When the brittleness number is increased to 0.3, the beam collapses by flexural failure at the midspan crack, although an increment in nondimensional shear force from 0.18 to 0.25 is observed and new neighboring cracks develop. If the brittleness number is increased to 0.4 (Fig. 7(c)), flexural and diagonal tension failure occur at the same load level. In fact, the minimum of the maxima of the crack propagation curves coincides with the slope discontinuity (yielding) of the curve for $\alpha_0 = 1$ (central crack). For higher values of the brittleness number (Fig. 7(d)), flexural failure needs a higher shear ($\alpha_0 = 1$, $V_F = 0.80$) than diagonal tension failure ($\alpha_0 = 0.6$, $V_F = 0.33$). Therefore, as N_P is increased, the failure mode shows a transition from flexural to shear.

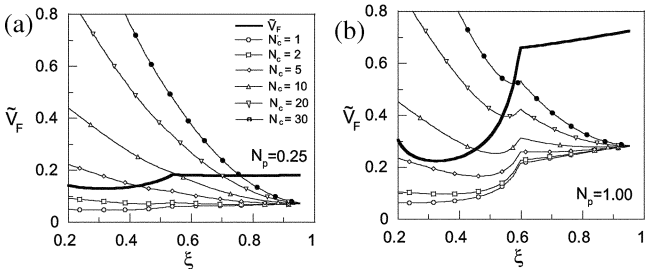

Fig. 6—Influence of N_C *on computed shear as function of crack depth: (a)* $N_P = 0.25$*; and (b)* $N_P = 1.0$*.*

Figure 8 shows a sketch of all the failure mode transitions in RC elements. An increase in the brittleness number N_P (Eq. (6)) can be interpreted as: 1) an increase in the reinforcement area, transition *d-e*; 2) a decrease in the scale with constant reinforcement area, transition *a-e*; and 3) an increase in the scale with a constant reinforcement percentage, transition *g-e*.

The combined influence of the brittleness number N_P and of the slenderness λ_l on the failure mode is shown in Fig. 9. Two transition curves from flexural to shear failure are reported for two values of the crack trajectory exponent, $\mu = 4$ and $\mu = 6$. These curves separate the regions of couples of values $N_P - \lambda_l$ giving flexural or shear failure. The two parameters controlling the model—that is, the slenderness λ_l

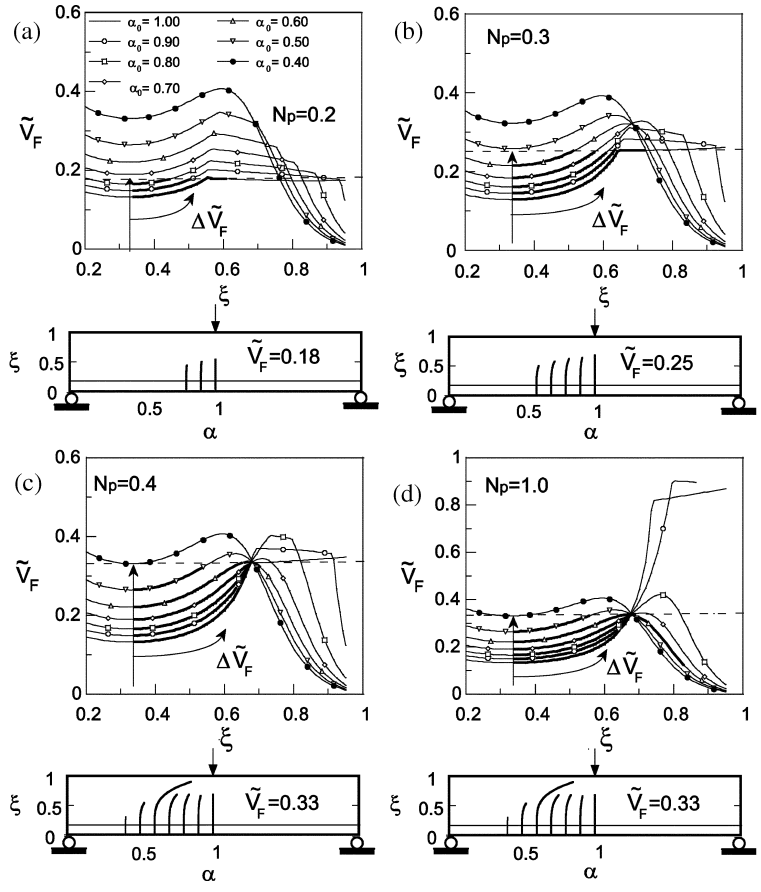

Fig. 7—Transition from flexural to diagonal tension failure by varying N_P*: (a)* $N_P = 0.2$*; (b)* $N_P = 0.3$*; (c)* $N_P = 0.4$*; and (d)* $N_P = 1.0$*.*

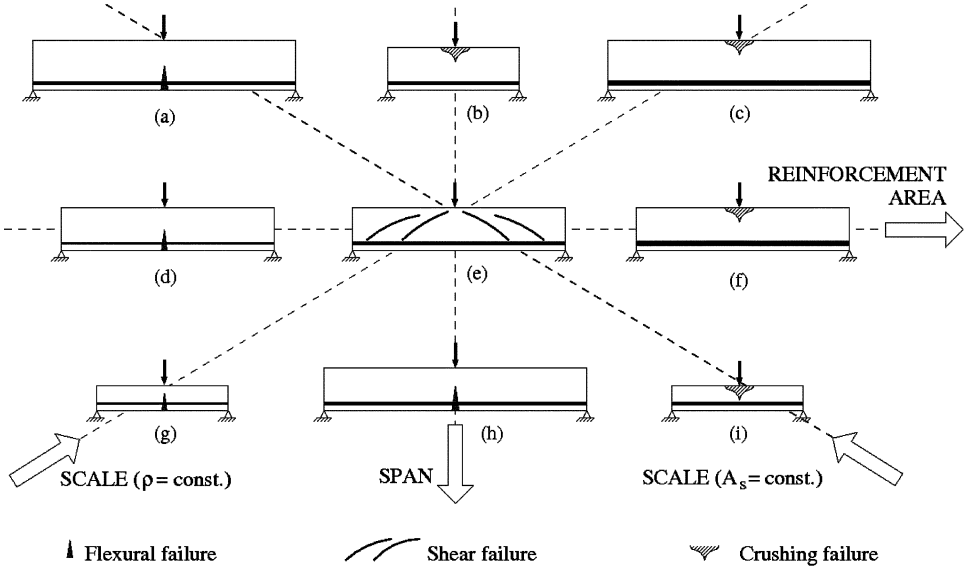

Fig. 8—Global scheme illustrating failure mode transitions.

and the brittleness number N_P—rule the transition between the failure modes demonstrating the transition *e-h* in Fig. 8. Depending on the material properties, as the critical shear crack progressively reduces the size of the ligament in the extrados of the beam, concrete crushing failure may take place, transition *e-b*.

To discuss the right part of the transition diagram (Fig. 8), crushing failure is considered and the behavior depends on the parameters N_P, N_C, and λ_l.

In Fig. 10(a), the transition is shown by varying N_P. The shear $\tilde{V}_F$ at yielding increases with N_P (Points A and D). The transition from flexural to crushing failure is apparent in Fig. 10(a): for $N_P = 0.2$, yielding precedes crushing, whereas for $N_P = 0.6$, crushing precedes yielding. In Fig. 10(b), the transition can be observed from the failure shear of the two mechanisms. For low values of N_P, failure is by steel yielding. For $N_P \cong 0.3$, the transition takes place and the shear of crushing failure is lower. Physically, this transition appears when the reinforcement ratio ρ is increased and the remaining parameters are kept constant, resulting in transition *d-e-f* in the scheme of Fig. 8. Note that in Fig. 10(b), before the transitional value $N_P \cong 0.3$, the two mechanisms (yielding and crushing) have apparently the same failure load. This is due to the fact that when yielding occurs, the $\tilde{V}_F$ versus ξ curve is almost horizontal. Therefore, concrete crushing is attained almost at the same load level as yielding, although at a considerably higher crack depth (refer to Fig. 10(a)), that is, yielding precedes crushing.

Another transition can be shown as the beam is scaled keeping ρ constant (transition *g-e-c* in Fig. 8). By the definitions of N_P and N_C, this condition can be expressed by a constant ratio N_C/N_P. Curves for $N_C/N_P = 50$ are reported in Fig. 11. For the ratio being constant, increasing N_P implies increasing N_C; therefore, both the loads for flexural/shear collapse (controlled by N_P), as well as the load for crushing collapse (controlled by N_C) increase but with different rates (Fig. 11(b)); and the failure mode transition occurs at $N_P \cong 0.4$.

Finally, the size effect is analyzed in the hypothesis that the reinforcement area A_s is constant, implying that the ratio N_C/N_P is proportional to the cross-section depth h (Fig. 12(a)). The abscissas of the graph (Fig. 12(b)) report

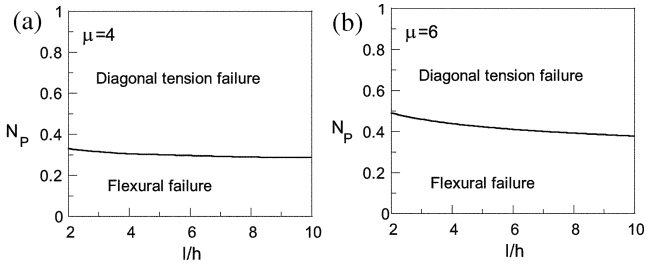

Fig. 9—Transition from flexural to diagonal tension failure by varying N_P *and* λ_l*: (a)* $\mu = 4$*; and (b)* $\mu = 6$*.*

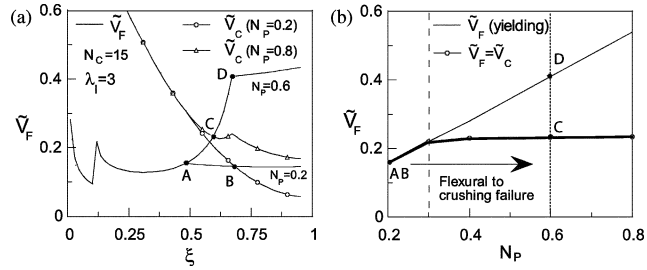

Fig. 10—Transition from flexural to crushing failure: (a) V_F *versus* ξ*; and (b)* V_F *versus* N_P*.*

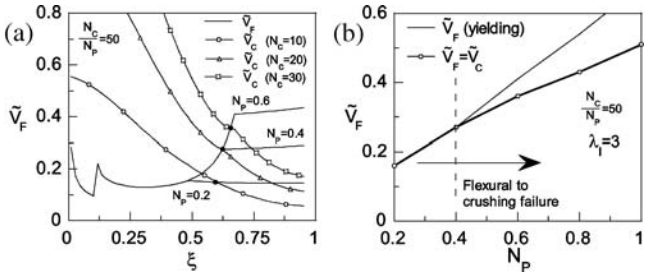

Fig. 11—Transition from flexural/shear to crushing failure assuming ratio $N_P/N_C = 50$*, corresponding to variation in scale with constant reinforcement percentage* ρ*: (a)* $\tilde{V}_F$ *versus* ξ *(black dots representing collapse load); and (b)* V_F *versus* N_P*.*

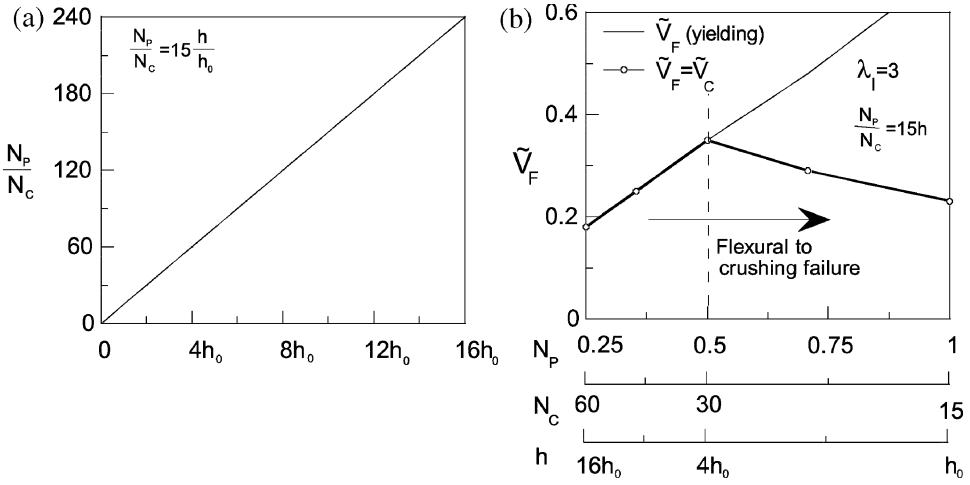

Fig. 12—Transition from flexural to crushing failure. Ratio N_P/N_C *is assumed proportional to beam height, corresponding (a) to variation in scale with constant area* A_s. *On the right (b),* V_F *versus* N_P, *with abscissas reporting three related quantities* N_P, N_C, *and* h ($h_0 = 1$).

the brittleness numbers N_P and N_C, as well as the beam depth h. An increase in N_P implies a decrease in N_C and h. For low values of N_P, the yielding load is lower than the crushing load. As the beam depth decreases, a transition point exists where the crushing load becomes lower. This illustrates the transition *a-e-i* in Fig. 8.

The scheme in Fig. 8 summarizes the failure transitions from flexural to crushing predicted by the model.

The transitions to crushing can take place when there is: 1) an increase in the reinforcement area, transition *d-e-f*; 2) an increase in the size-scale with constant reinforcement percentage, transition *g-e-c*; 3) a decrease in the size-scale with constant reinforcement area, transition *a-e-i*; and 4) a decrease in the span, transition *h-e-b*.

In some cases, depending on material and geometrical properties, the intermediate transition through (*e*) may be skipped and a direct transition from yielding to crushing can be observed.

CONCLUSIONS

In this study, a new model is introduced to analyze flexural, shear, and crushing failure with a unified approach. The model shows failure mode transitions by varying the controlling nondimensional parameters and demonstrates size effects in the mechanical behavior of RC beams. The following main points are observed:

1. Diagonal tension failure is due to an unstable cracking process. Depending on the values of the brittleness number and the beam slenderness, the propagation of shear cracks originated along the beam span requires lower loads compared to cracks close to the beam midspan (flexural cracks) or cracks originating near the support;

2. The size effect in the flexural to shear failure transition is governed by the brittleness number N_P; and

3. The size effect in the flexural/shear to crushing failure transition is ruled by the brittleness numbers N_P and N_C and by the slenderness λ_l.

ACKNOWLEDGMENTS

The second author gratefully acknowledges the financial support provided by the Ministerio de Educación y Ciencia, Spain (under Grant No. MAT2003-00843) and by the Junta de Comunidades de Castilla-La Mancha, Spain (under Grant No. PAI08-0196-8210).

The first and third authors gratefully acknowledge the financial support of the Ministry of University and Research (under the PRIN projects 2003, 2005, and 2008).

NOTATION

A_s	=	bar cross-sectional area
a	=	crack depth
b	=	beam width
c	=	reinforcement cover
E	=	concrete Young's modulus
h	=	beam depth
K_{IP}	=	stress-intensity factor due to closing force at reinforcement bars
K_{IV}	=	stress-intensity factor associated to shear force
K_K	=	concrete toughness
K_1	=	stress-intensity factor at crack tip
l	=	shear span
N_C	=	brittleness number for crushing failure
N_P	=	Carpinteri's brittleness number (bending)
P	=	reinforcement reaction
P_P	=	maximum for bridging reinforcement reaction
$\tilde{P}$	=	nondimensional bar reaction
V	=	applied shear force
V_C	=	shear of crushing failure
V_F	=	shear of crack propagation
$\tilde{V}$	=	nondimensional applied shear
$\tilde{V}_C$	=	nondimensional shear of crushing failure
$\tilde{V}_F$	=	nondimensional shear of crack propagation
$\tilde{V}_P$	=	nondimensional shear of bar yielding or slippage
w	=	crack opening at reinforcement level
$\tilde{w}$	=	nondimensional crack opening at reinforcement level
x	=	crack tip horizontal position
x_0	=	crack mouth horizontal position
α	=	nondimensional horizontal distance from support to crack tip
α_0	=	nondimensional initial crack mouth position
γ	=	trajectory angle
λ_l	=	shear span slenderness ratio
μ	=	trajectory exponent
ρ	=	reinforcement area percentage
σ_c	=	stress at beam extrados
σ_{cu}	=	concrete crushing strength
σ_s	=	bar traction stress
σ_{y_P}	=	minimum between yielding and sliding stress for bars
σ_{V^C}	=	stress at extrados due to reinforced reaction
σ_C	=	stress at extrados due to shear applied
ξ	=	nondimensional crack depth
ζ	=	nondimensional reinforcement cover

REFERENCES

1. Kani, G. N. J., "The Riddle of Shear Failure and its Solution," ACI JOURNAL, *Proceedings* V. 61, No. 4, Apr. 1964, pp. 441-467.

2. Gustafsson, P.-J., "Fracture Mechanics Studies of Non-Yielding Materials like Concrete: Modeling of Tensile Fracture and Applied Strength Analyses," *Report* No. TVBM-1007, Division of Buildings Materials, Lund Institute of Technology, Lund, Sweden, 1985, 422 pp.

3. Gustafsson, P.-J., and Hillerborg, A., "Sensitivity in Shear Strength of Longitudinally Reinforced Concrete Beams to Fracture Energy of Concrete," *ACI Structural Journal*, V. 85, No. 3, May-June 1988, pp. 286-294.

4. Niwa, J., "Size Effect Analyses for Flexural Strength of Concrete Beams Using Non-Linear Rod Element," *Proceedings of JCI*, V. 15, No. 2, 1993, pp. 75-80.

5. Niwa, J., "Size Effect in Shear of Concrete Beams Predicted by Fracture Mechanics," *CEB Bulletin d'Information*, No. 137, Comité Euro-International du Béton (CEB), Lausanne, Switzerland, 1997, pp. 147-158.

6. Jenq, Y. S., and Shah, S. P., "Shear Resistance of Reinforced Concrete Beams—A Fracture Mechanics Approach," *Fracture Mechanics: Applications to Concrete*, SP-118, V. Li and Z. P. Bažant, eds., American Concrete Institute, Farmington Hills, MI, 1990, pp. 237-258.

7. Carpinteri, A., "A Fracture Mechanics Model for Reinforced Concrete Collapse," *Proceedings of the I.A.B.S.E. Colloquium on Advanced Mechanics of Reinforced Concrete*, Delft, the Netherlands, 1981, pp. 17-30.

8. Carpinteri, A., "Stability of Fracturing Process in RC beams," *Journal of Structural Engineering*, ASCE, V. 110, 1984, pp. 544-558.

9. So, K. O., and Karihaloo, B., "Shear Capacity of Longitudinally Reinforced Beams—A Fracture Mechanics Approach," *ACI Structural Journal*, V. 90, No. 6, Nov.-Dec. 1993, pp. 591-600.

10. Karihaloo, B. L., "Approximate Fracture Mechanical Approach to the Prediction of Ultimate Shear Strength of RC Beams," *Fracture Mechanics of Concrete Structures*, F. H. Wittmann, ed., Aedificatio Publishers, Freiburg, Germany, 1995, pp. 1111-1123.

11. Bosco, C.; Carpinteri, A.; and Debernardi, P. G., "Minimum Reinforcement in High-Strength Concrete," *Journal of Structural Engineering*, ASCE, V. 116, No. 2, 1990, pp. 228-236.

12. Bosco, B., and Carpinteri, A., "Fracture Mechanics Evaluation of Minimum Reinforcement in Concrete Structures," *Applications of Fracture Mechanics to Reinforced Concrete*, A. Carpinteri, ed., Elsevier Applied Science, London, UK, 1992, pp. 347-377.

13. Bosco, C., and Carpinteri, A., "Softening and Snap-Through Behavior of Reinforced Elements," *Journal of Engineering Mechanics*, ASCE, V. 118, No. 8, 1992, pp. 1564-1577.

14. Carpinteri, A., "Minimum Reinforcement in Concrete Members," ESIS Publications, V. 24, Elsevier, London, UK, 1999, 30 pp.

15. Carpinteri, A., and Massabò, R., "Bridged versus Cohesive Crack in the Flexural Behavior of Brittle-Matrix Composites," *International Journal of Fracture*, V. 81, No. 2, 1996, pp. 125-145.

16. Carpinteri, A., and Massabò, R., "Continuous versus Discontinuous Bridged-Crack Model for Fiber-Reinforced Materials in Flexure," *International Journal of Solids and Structures*, V. 34, No. 21, 1997, pp. 2321-2338.

17. Carpinteri, A.; Ferro, G.; and Ventura, G., "Size Effects on Flexural Response of Reinforced Concrete Elements with a Nonlinear Matrix," *Engineering Fracture Mechanics*, V. 70, 2003, pp. 995-1013.

18. Carpinteri, A.; Ferro, G.; and Ventura, G., "Double Brittle-to-Ductile Transition in Bending of Fibre-Reinforced Concrete Beams with Rebars," *International Journal for Numerical and Analytical Methods in Geomechanics*, V. 28, 2004, pp. 737-756.

19. Tada, H.; Paris, P.; and Irwin, G., *The Stress Analyses of Cracks Handbook*, Paris Productions Incorporated (and Del Research Corporation), 1963, 542 pp.

20. Carpinteri, A.; Carmona, J. R.; and Ventura, G., "Flexural, Shear and Crushing Failure Transitions in Reinforced Concrete Beams—Part 2: Experimental Validation," *ACI Structural Journal*, V. 108, No. 3, May-June 2011, pp. 286-293.

21. RILEM TC 50-FCM, "Determination of the Fracture Energy of Mortar and Concrete by Means of the Three-Point Bend Test on Notched Beams," *Materials and Structures*, V. 18, 1985, pp. 287-290.

22. RILEM TC 89-FMT, "Determination of Fracture Parameters of Plain Concrete Using Three-Point Bend Tests," *Materials and Structures*, V. 23, 1990, pp. 457-460.

23. Abdalla, H., and Karihaloo, B., "Determination of Size Independent Specific Fracture Energy of Concrete from Three-Point Bend and Wedge Splitting Tests," *Magazine of Concrete Research*, V. 55, 2003, pp. 133-141.

24. Karihaloo, B., and Abdalla, H., "A Simple Method for Determining the True Specific Fracture Energy of Concrete," *Magazine of Concrete Research*, V. 55, 2003, pp. 471-481.

25. Portela, A., and Aliabadi, M. H., "Crack Growth Analysis Using Boundary Elements," *Computational Mechanics Publications*, Southampton, UK, 1992, 50 pp.

26. Carmona, J. R.; Ruiz, G.; and del Viso, J. R., "Mixed-Mode Crack Propagation through Reinforced Concrete," *Engineering Fracture Mechanics*, V. 74, 2007, pp. 2788-2809.

27. Carmona, J. R., "Study of Cracking Processes in Reinforced Concrete Elements," PhD thesis, Department of Applied Mechanics, Universidad de Castilla La Mancha, Ciudad Real, Spain, 2006, 215 pp.

28. Kim, W., and White, R. N., "Shear-Critical Cracking in Slender Reinforced Concrete Beams," *ACI Structural Journal*, V. 96, No. 5, Sept.-Oct. 1999, pp. 757-765.

29. Kim, W., and White, R. N., "Hypothesis for Localized Horizontal Shearing Failure Mechanism of Slender RC Beams," *Journal of Structural Engineering*, ASCE, V. 125, No. 10, 1999, pp. 1126-1135.